Improved coronary calcium detection and quantification with low-dose full field-of-view photon-counting CT

van der Werf, N R; Rodesch, P A; Si-Mohamed, S; van Hamersvelt, R W; Greuter, M J W; Leiner, T; Boussel, L; Willemink, M J; Douek, P

Published in:
European Radiology

DOI:
10.1007/s00330-021-08421-8

European Radiology
https://doi.org/10.1007/s00330-021-08421-8

CARDIAC

Improved coronary calcium detection and quantification with low-dose full field-of-view photon-counting CT: a phantom study

N. R. van der Werf[1,2] · P. A. Rodesch[3,4] · S. Si-Mohamed[3,4] · R. W. van Hamersvelt[1] · M. J. W. Greuter[5] · T. Leiner[1] · L. Boussel[3,4] · M. J. Willemink[6] · P. Douek[3,4]

Received: 31 August 2021 / Revised: 31 August 2021 / Accepted: 17 October 2021

Abstract

Objective The aim of the current study was to systematically assess coronary artery calcium (CAC) detection and quantification for spectral photon-counting CT (SPCCT) in comparison to conventional CT and, in addition, to evaluate the possibility of radiation dose reduction.

Methods Routine clinical CAC CT protocols were used for data acquisition and reconstruction of two CAC containing cylindrical inserts which were positioned within an anthropomorphic thorax phantom. In addition, data was acquired at 50% lower radiation dose by reducing tube current, and slice thickness was decreased. Calcifications were considered detectable when three adjacent voxels exceeded the CAC scoring threshold of 130 Hounsfield units (HU). Quantification of CAC (as volume and mass score) was assessed by comparison with known physical quantities.

Results In comparison with CT, SPCCT detected 33% and 7% more calcifications for the small and large phantoms, respectively. At reduced radiation dose and reduced slice thickness, small phantom CAC detection increased by 108% and 150% for CT and SPCCT, respectively. For the large phantom size, noise levels interfered with CAC detection. Although comparable between CT and SPCCT, routine protocols CAC quantification showed large deviations (up to 134%) from physical CAC volume. At reduced radiation dose and slice thickness, physical volume overestimations decreased to 96% and 72% for CT and SPCCT, respectively. In comparison with volume scores, mass score deviations from physical quantities were smaller.

Conclusion CAC detection on SPCCT is superior to CT, and was even preserved at a reduced radiation dose. Furthermore, SPCCT allows for improved physical volume estimation.

Key Points

• *In comparison with conventional CT, increased coronary artery calcium detection (up to 156%) for spectral photon-counting CT was found, even at 50% radiation dose reduction.*

• *Spectral photon-counting CT can more accurately measure physical volumes than conventional CT, especially at reduced slice thickness and for high-density coronary artery calcium.*

• *For both conventional and spectral photon-counting CT, reduced slice thickness reconstructions result in more accurate physical mass approximation.*

Keywords X-ray computed tomography · Calcium · Coronary vessels · Imaging phantoms · Radiation dosage

N.R. van der Werf and P.A. Rodesch contributed equally to this work.

✉ N. R. van der Werf
n.vanderwerf@erasmusmc.nl

[1] Department of Radiology, University Medical Center Utrecht, Utrecht, The Netherlands

[2] Department of Radiology & Nuclear Medicine, Erasmus University Medical Center, Rotterdam, The Netherlands

[3] Louis Pradel Cardiology Hospital, Hospices Civils de Lyon, Lyon, France

[4] Univ Lyon, INSA-Lyon, Université Claude Bernard Lyon 1, UJM-Saint Etienne, CNRS, Inserm, CREATIS UMR 5220, U1206 Lyon, France

[5] Department of Radiology, University of Groningen, University Medical Center Groningen, Groningen, The Netherlands

[6] Department of Radiology, Stanford University School of Medicine, Stanford, CA, USA

Published online: 08 January 2022

Abbreviations

BAS	Background Agatston score
CAC	Coronary artery calcification
CTDIvol	Volumetric CT dose index
DLCT	Dual-layer CT
EID	Energy integrating detector
HA	Hydroxyapatite
HU	Hounsfield units
IR	Iterative reconstruction
PCD	Photon-counting detector
ROI	Region of interest
SD	Standard deviation
SPCCT	Spectral photon-counting CT

Introduction

All major computed tomography (CT) manufacturers are currently developing spectral photon-counting CT (SPCCT) systems [1, 2]. The difference with conventional CT is the fundamentally improved detector technology. Conventional CT uses energy-integrating detectors (EID), while PCCT uses photon-counting detectors (PCD). With PCD, individual photons are counted within predefined energy specific bins characterized by thresholds. This technology reduces the influence of electronic noise by setting the lowest threshold above the electronic noise [2]. Because electronic noise is superimposed on each pulse, when the widths of the energy bins are set sufficiently wide, the impact of electronic noise is only minor, reducing the resulting total image noise [3–5].

With conventional EID, X-ray photons are converted to visual light photons, which may affect neighboring detector pixels. This phenomenon is called optical cross talk, which is limited by the highly reflective septa between EID pixels. With PCD, X-ray photons are directly converted into an electric signal without conversion to visual light photons. Therefore, no reflective septa are needed between PCD pixels, allowing for smaller detector pixels. Furthermore, small detector pixels are required for SPCCT to allow for individual photons to be counted without suffering from pulse pile-up effects [6–8]. This decreased detector pixel size enhances spatial resolution for SPCCT in comparison with conventional CT, both in-plane and through-plane. In turn, increased spatial resolution results in a decrease of partial volume effects and blooming artefacts, which are especially important for high-contrast materials such as iodinated contrast, bone, and calcium.

An important use case for these major improvements in CT technology is coronary artery calcium (CAC) detection and quantification [9]. The highly significant association between CAC as characterized with CT, total coronary atherosclerosis burden, and future adverse cardiovascular events is well known [10]. Moreover, ischemic heart disease caused by coronary plaque remains, according to the World Health Organization, the main cause of death worldwide [11]. Evaluation of CAC detection and quantification with CT imaging are thus recommended in guidelines for clinical risk prediction in appropriately selected asymptomatic individuals, resulting in a high number of CT examinations for CAC assessment [12–14]. In this screening setting, accurate and precise CAC assessment at a low radiation dose is therefore key. Clinically, CAC is assessed according to the Agatston methodology (120 kVp, 3 mm slice thickness, 130 Hounsfield units (HU) CAC threshold) [15]. For routine protocols, based on the Agatston methodology, SPCCT outcome is in agreement with conventional CT [16]. In addition to the Agatston score, newer CAC metrics have been introduced, which are related to the physical measures of volume and mass [17, 18]. These metrics have been shown to improve reproducibility of CAC assessment with EID CT [19–21].

With current conventional CT systems, the accuracy of CAC quantification is affected by blooming artefacts around CAC, which increases inter- and intra-scan variability [9]. The effect of blooming on different CAC densities differs, with underestimation and overestimation of low and high density CAC, respectively. Moreover, due to partial volume averaging effects, small CAC may not be detected, as the conventional Agatston scoring threshold of 130 HU may not be reached. A systematic assessment of the influence of PCD in comparison with EID for CAC detection and quantification of different densities of CAC is lacking.

Furthermore, due to the reduced impact of electronic noise on SPCCT images, data acquisition for CAC assessment could potentially be performed at a reduced radiation dose, while maintaining image quality in comparison with EID [2, 4, 22]. The combination of SPCCT acquisitions at a reduced radiation dose, in combination with iterative reconstruction (IR), could theoretically further decrease radiation dose burden. Several studies indicated that CT radiation dose reduction with the use of IR did not affect CAC scores compared to routine radiation dose and reconstruction [23–30]. However, for these studies, images were acquired with conventional EID CT. The impact of IR on CAC scores for images acquired with PCD remains unknown.

The aim of the current study is therefore twofold. First, we systematically assess CAC detection and quantification for SPCCT in comparison with conventional CT, and second, we evaluate the possibility of dose reduction.

Materials and methods

Phantom

Anthropomorphic phantoms were used to assess the potential of SPCCT to improve CAC detectability and quantification. We used two setups, which both consisted of an anthropomorphic (cardio)thoracic CT phantom (QRM Thorax, QRM GmbH), in combination with a task-specific cylindrical insert. For the detectability task, the D100 (D100, QRM GmbH) insert was used. This insert contained 100 cylindrical calcifications, divided over four planes, where each plane consisted of a 5 × 5 matrix of calcifications. The diameter and length of all calcifications were identical, and ranged from 0.5 to 2.0 mm. The densities of the calcifications ranged from 90 to 540 mg hydroxyapatite (HA) cm^{-3}. The quantification task was assessed with the Cardiac Calcification Insert (CCI, QRM GmbH), which contained three cylindrical (5.0 mm in length and diameter) calcifications with densities of 800, 400, and 200 $mgHAcm^{-3}$, designated as high, medium, and low density, respectively [17, 31]. The CCI insert also contained two large calibration rods, consisting of water-equivalent and 200 $mgHAcm^{-3}$ materials, which were used to calculate a mass calibration factor as described by McCollough et al. [17].

To further assess the influence of radiation dose on CAC scoring with SPCCT, two phantom sizes were assessed by adding a tissue-equivalent extension ring (QRM Extension Ring, QRM GmbH) to the anthropomorphic thorax phantom. The resulting dimensions of the phantom were 300 mm × 200 mm without an extension ring, and 400 mm × 300 mm with an extension ring, which simulates a small- and a large-sized patient, respectively [17].

Acquisition and reconstruction parameters

Data acquisition was performed on two CT systems from one manufacturer. First, a conventional dual-layer CT (DLCT) (IQon Spectral CT, Philips Healthcare) was used, which uses EID for image acquisition. Second, a prototype full field-of-view SPCCT system (Spectral Photon Counting CT, Philips Healthcare) was used, which uses novel PCD technology for image acquisition.

For both phantom sizes, routine clinical CAC protocols recommended by the vendor for conventional CT were used on both CT systems (Table 1). In addition to standard reconstruction parameters (3 mm slice thickness and IR level 0), raw data was also reconstructed at 1-mm slice thickness, and with IR levels 3 and 5. Furthermore, to assess the potential of radiation dose reduction, tube currents were reduced by 50% for each phantom size. Each scan was repeated five times, with manual repositioning between each scan (2 mm translation, 2° rotation).

Table 1 Routine clinical CAC acquisition and reconstruction parameters for DLCT. SPCCT parameters were matched to this as closely as possible

Parameter	DLCT	SPCCT
CT system	IQon	SPCCT
Technique	Sequential	Sequential
Tube voltage (kVp)	120	120
Tube current time product (mAs)	Small phantom: 40[1] Large phantom: 80[1]	Small phantom: 40[1] Large phantom: 80[1]
Automatic exposure correction	Off	Off
Focal spot	Standard	Small[2]
Collimation (mm)	64 × 0.625	64 × 0.275
Field of View (mm)	220	220
Rotation time (s)	0.27	0.33
Slice thickness, increment (mm)	3.0 – 3.0	3.0 – 3.0
Reconstruction kernel	IQon-Std-B	SPCCT-Std-B[3]
Matrix size (pixels)	512 × 512	512 × 512
Reconstruction (iDose level)	0	0
Volume CT dose index (mGy)	Small phantom: 4.5 Large phantom: 9.4	Small phantom: 4.0 Large phantom: 8.1

[1]Reference tube current from routine clinical protocol for DLCT

[2]The small focal spot is the only available option for the current clinical SPCCT prototype

[3]Despite differences in detector pixel size, reconstruction kernel and reconstruction algorithm for SPCCT, reconstruction parameters for SPCCT were optimized by the manufacturer to get comparable results as with DLCT

DLCT, dual-layer computed tomography; *SPCCT*, spectral photon-counting computed tomography

Analysis

For all reconstructions, CAC scores were determined with the use of a previously validated, in-house developed open-source Python script (Python version 3.7) [32, 33]. To obtain CAC scores which were equal to CAC scores calculated with the vendor-specific software, vendor-specific implementations of both the volume and mass score were used [15, 18]. For both metrics, a CAC scoring threshold of 130 HU was used. Furthermore, only groups of connected voxels with a minimum in-plane area of 0.5 mm^2 were taken into consideration for CAC scoring. For the used reconstruction parameters, with a reconstructed pixel spacing of 0.43×0.43 mm^2 (220 mm field-of-view and 512×512 matrix), this resulted in a minimum of 3 horizontally or vertically connected voxels. Finally, no interpolation was used for the volume score calculation.

Image noise (standard deviation [SD]) was determined in a large square (128×128 voxels) region-of-interest (ROI) of uniform background material. In addition, a false-positives analysis was performed, to assess the extent of erroneous detection of CAC in locations where no CAC was present. False positives were defined as groups of voxels > 0.5 mm^2 with CT values exceeding 130 HU in the D100 phantom with the largest and highest density CAC, where the known CAC locations were masked [32, 33]. This resulted in a background Agatston score (BAS). Reconstructions with BAS > 0 were defined as non-diagnostic for CAC detection assessment, as it was uncertain if CAC was detected or if a CAC score was calculated based on only noise. As a result, all repetitions of the D100 insert with BAS > 0 were discarded for CAC detection analysis.

Due to the large size of the CCI calcifications, CAC localization for this insert was not hampered by reconstructions with BAS > 0. Therefore, all reconstructions of the CCI insert were taken into consideration for CAC quantification. Reconstructions with BAS > 0 could result in a slight increase in resulting CAC scores.

For all reconstructions, CAC scores were determined for each of the 100 calcifications of the D100 insert. For each combination of CT system, phantom size, IR level, slice thickness, and radiation dose level, detectability was defined as the ability to calculate a CAC score for each individual calcification.

For each calcification of the CCI insert, volume and mass scores were determined. For each combination of CT system, phantom size, IR level, slice thickness, radiation dose level, and CAC density, CAC scores were compared with the physical values, a volume of 96.2 mm^3 for all calcifications, and mass of 78.5, 39.3, and 19.6 mg for high-, medium-, and low-density CAC, respectively. Over- and/or underestimations of physical volume and mass were calculated by dividing the calculated value by the physical value.

Results

Reference volume CT dose indices ($CTDI_{vol}$) for the small phantom were 4.5 and 4.0 mGy, for DLCT and SPCCT, respectively. For the large phantom, reference $CTDI_{vol}$ was 9.4 and 8.1 mGy, respectively (Table 1). Resulting image noise levels for all radiation dose levels are shown in Table 2. Several combinations of phantom size, radiation dose reduction, and IR level resulted in false-positive CAC detection (BAS > 0) (Table 2). The number of repetitions

Table 2 Image noise (SD) levels in HU, presented as median (total range) for both DLCT and SPCCT, both phantom sizes, three IR levels, and both radiation dose levels. Image noise levels which lead to BAS > 0 for one or more repetitions are indicated in italics

CT system	Phantom size	IR level	3 mm slice thickness		1 mm slice thickness	
			100% dose	50% dose	100% dose	50% dose
DLCT	Small	0	15.4 (15.2–16.9)	22.3 (14.7–23.0)	28.4 (17.7–29.1)	*38.8 (24.4–40.1)*
		3	8.2 (8.0–13.3)	17.4 (11.5–18.1)	22.2 (13.8–22.7)	30.2 (19.0–31.2)
		5	6.7 (6.7–11.0)	14.3 (9.5–14.9)	18.1 (11.3–18.7)	24.6 (15.5–25.6)
	Large	0	*28.8 (27.7–33.1)*	*41.6 (37.9–43.2)*	*49.0 (48.4–53.0)*	*66.7 (66.2–70.2)*
		3	22.7 (21.8–27.1)	*33.0 (29.7–34.4)*	*38.1 (37.7–42.1)*	*52.0 (51.7–55.2)*
		5	18.8 (17.9–23.4)	*27.6 (24.5–29.3)*	*31.2 (30.9–35.2)*	*42.7 (42.2–45.6)*
SPCCT	Small	0	14.1 (13.9–14.3)	19.8 (19.2–21.3)	23.5 (23.0–23.9)	33.1 (32.4–37.6)
		3	11.3 (11.1–11.4)	15.8 (15.3–16.9)	18.5 (18.1–18.8)	26.0 (25.5–29.4)
		5	9.5 (9.3–9.6)	13.3 (12.9–14.1)	15.3 (15.0–15.6)	21.6 (21.2–24.2)
	Large	0	28.4 (28.1–28.8)	*41.3 (40.5–44.4)*	*46.4 (46.1–47.3)*	*70.5 (67.3–78.4)*
		3	22.7 (22.5–23.1)	*33.0 (32.4–35.3)*	37.0 (36.3–37.3)	*55.5 (53.0–56.3)*
		5	19.1 (18.9–19.5)	27.8 (27.3–29.6)	30.8 (30.1–31.0)	*46.4 (44.5–46.7)*

DLCT, dual-layer CT; *SPCCT*, spectral photon-counting CT; *BAS*, background Agatston score; *IR*, iterative reconstruction

Table 3 Number of repetitions, out of the total of five, which did not lead to false positives (BAS = 0). These repetitions were considered to be of diagnostic quality for CAC detection purposes

CT system	Phantom size	IR level	3-mm slice thickness		1-mm slice thickness	
			100% dose	50% dose	100% dose	50% dose
DLCT	Small	0	5	5	5	2
		3	5	5	5	5
		5	5	5	5	5
	Large	0	4	3	1	0
		3	5	2	0	0
		5	5	3	0	0
SPCCT	Small	0	5	5	5	5
		3	5	5	5	5
		5	5	5	5	5
	Large	0	5	2	0	0
		3	5	4	5	0
		5	5	5	5	0

DLCT, dual-layer CT; *SPCCT*, spectral photon-counting CT; *BAS*, background Agatston score; *IR*, iterative reconstruction

which were of diagnostic quality for CAC detection is shown in Table 3. For these repetitions, BAS did not exceed 0 and it was certain that noise did not lead to false-positive CAC detection.

Detectability results (D100 insert)

Representative images and the total number of detected calcifications for both CT systems, phantom sizes, slice thickness, and radiation dose levels are shown in Figs. 1 and 2, respectively. In comparison with DLCT, SPCCT showed an overall superior CAC detectability. For the routine clinical protocol (3 mm slice thickness, 100% radiation dose and IR level 0), DLCT detected a median (range) number of 12 (11–16) and 14 (13–16) out of 100 calcifications for the small and large phantoms, respectively. For SPCCT, CAC detection increased to 16 (14–23) and 15 (14–17), respectively.

At a reduced slice thickness of 1 mm, the median number of detected calcifications in the small phantom increased by 142% for DLCT and by 156% for SPCCT. For the large phantom, reduced slice thickness resulted in non-diagnostic image quality for CAC detection (BAS > 0) for DLCT for all reconstructions. For SPCCT, this was only the case when IR level 0 was used. However, changing IR level to 3 enabled satisfying image quality and increased median CAC detection by 127% for the large phantom in comparison with the routine clinical protocol.

At both reduced slice thickness and reduced radiation dose, noise levels were too high for the large phantom for both DLCT and SPCCT with all IR levels, resulting in non-diagnostic image quality for CAC detection (BAS > 0). For the small phantom, however, median CAC detection was still increased in comparison with 100% dose and 3-mm slice thickness when appropriate IR levels were selected (Fig. 2). For DLCT at 50% dose and 1-mm slice thickness with IR level 0, the median (range) number of detected calcifications was 25 (24–26), which is equal to an increased CAC detection of 108% in comparison with the routine clinical protocol. For SPCCT with IR level 0, the median (range) number of detected calcifications was 40 (39–44), which is equal to an increased CAC detection of 150% in comparison with the routine clinical protocol.

Quantification results (CCI insert)

Routine clinical CAC protocols (100% dose, 3 mm slice thickness, and IR level 0) resulted in comparable volume scores for the CCI insert between DLCT and SPCCT, independent of phantom size or CAC density (Figs. 3 and 4). However, especially for the high-density calcifications, large deviations from the physical volume of the calcifications were shown. For DLCT, small phantom volume scores from routine clinical protocols overestimated physical volume by (median (range)) 116% (110 to 157%), 62% (56 to 106%), and 21% (15 to 23%) for high, medium, and low CAC density, respectively. For SPCCT, small phantom volume scores overestimated physical CAC volume for routine clinical protocols by 134% (131 to 138%), 93% (50 to 96%), and 16% (7 to 24%) for high, medium, and low CAC density, respectively.

In comparison to volume scores, deviations from physical quantities were in general smaller for mass scores (Fig. 4). For DLCT, small phantom mass scores from routine clinical protocols deviated from physical mass by (median (range)) 9% (4 to 13%), − 5% (− 8 to 2%), and − 10% (− 18 to − 7%) for high, medium, and low CAC density, respectively. For SPCCT, small phantom mass scores deviated from physical

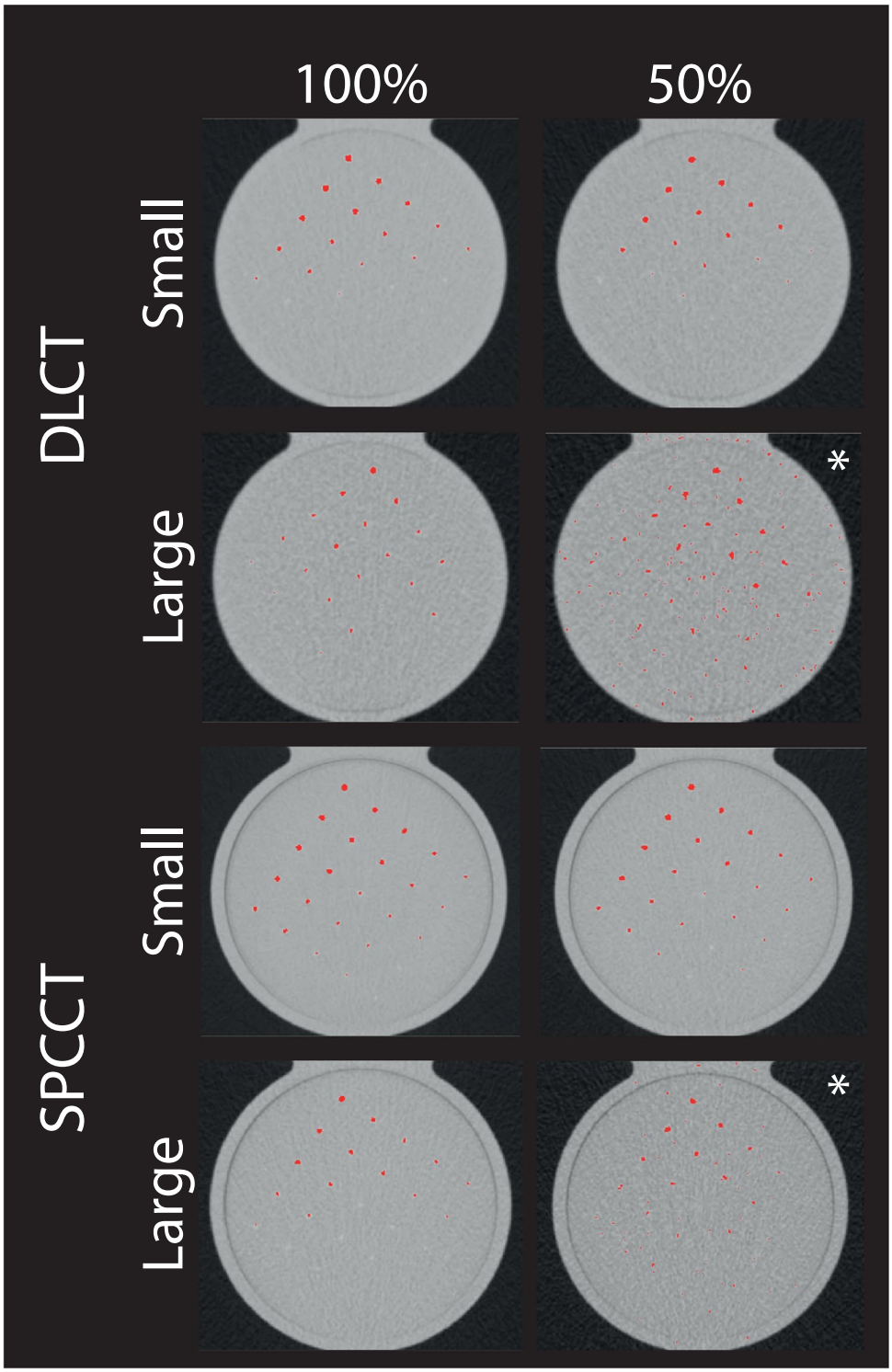

Fig. 1 Representative images for the D100 insert placed in the small and large phantoms, for DLCT and SPCCT for routine clinical protocols (100% radiation dose, IR level 0- and 3-mm slice thickness) and 50% reduced radiation dose. Voxels exceeding the CAC scoring threshold of 130 HU are indicated in red. An asterisk indicates reconstructions for which BAS > 0

CAC mass by 5% (2 to 7%), − 3% (− 7 to − 1%), and − 23% (− 27 to − 13%) for high, medium, and low CAC density, respectively.

The influence of radiation dose, IR levels, and phantom size on volume approximation was only minor (Fig. 3). However, reconstructions at reduced slice thickness reduced partial volume effects, and therefore improved volume scores substantially, in particular for high-density CAC and SPCCT. For DLCT at routine dose, 1-mm slice thickness, and IR level 0, small phantom volume scores were overestimated by 96% (91 to 101%), 57% (49 to 61%), and 20% (12 to 24%), again for high, medium, and low CAC density, respectively.

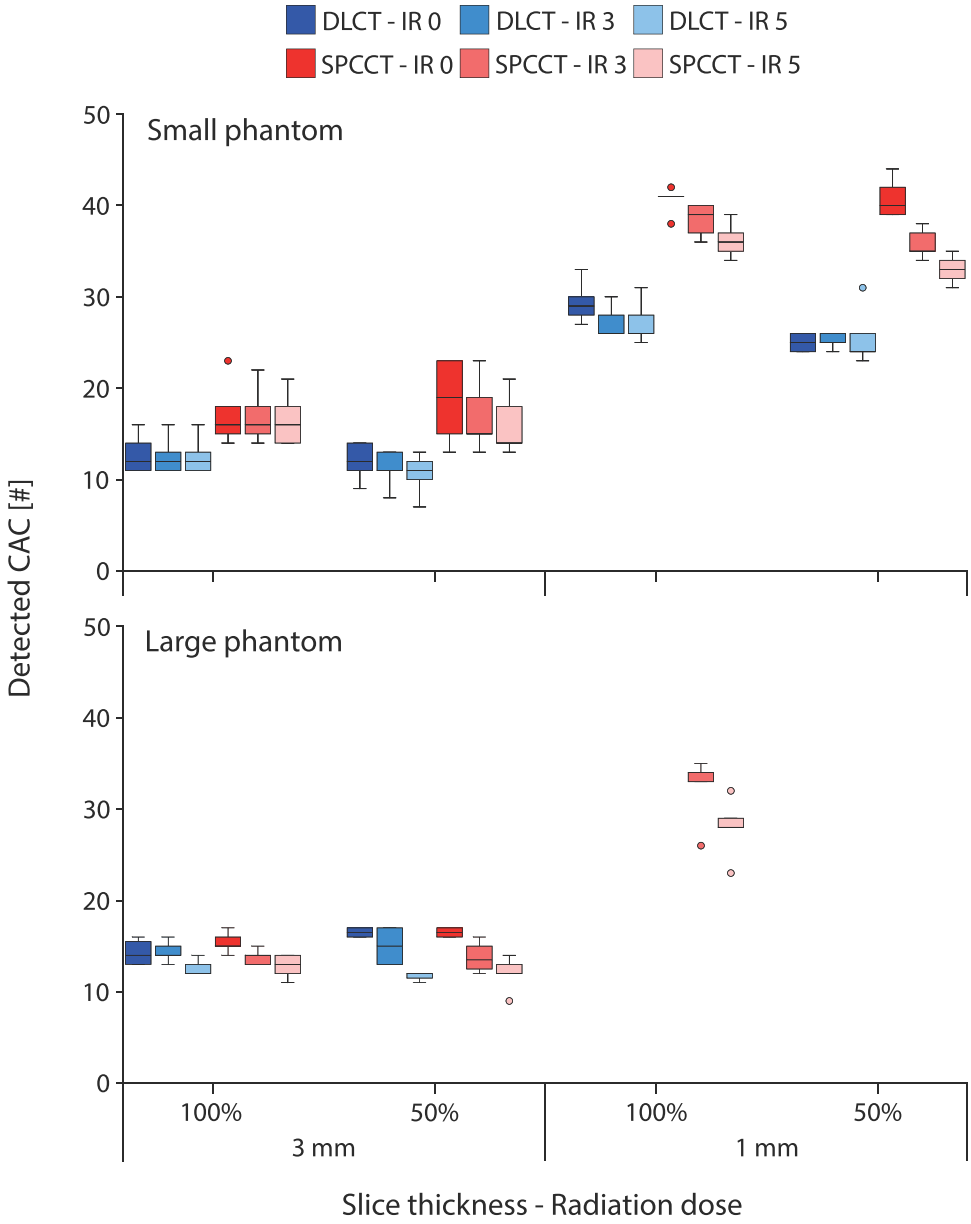

Fig. 2 Box and whisker for the total number of detected CAC from the 100 present CAC in the D100 insert for the small (upper) and large (lower) phantom sizes. Results are shown for both used slice thicknesses and radiation dose levels

For SPCCT, this volume overestimation was 72% (71 to 83%), 48% (35 to 50%), and 16% (12 to 22%). In comparison with DLCT, SPCCT showed superior physical volume depiction for all CAC densities at reduced slice thickness.

Physical mass approximation improved for reduced slice thickness for both CT systems and all CAC densities (Fig. 4). For both CT systems, the largest decrease in physical mass deviation was shown for the low-density CAC. DLCT small phantom deviation from physical mass at 1-mm slice thickness, 100% radiation dose, and IR level 0 in median (range) was 8% (7 to 14%), 1% (−1 to 5%), and −3% (−8 to −1%) for high, medium, and low CAC density, respectively. SPCCT mass scores deviated from physical mass by 4% (3 to 5%), 1% (−1 to 3%), and −8% (−9 to −7%) for high, medium, and low CAC density, respectively. Changes in physical mass approximation for changes in radiation dose for both CT systems, slice thickness, and IR were only minor.

Discussion

The current study shows superior CAC detectability for SPCCT in comparison with DLCT. SPCCT shows improved CAC detection (up to 156%) at reduced slice thickness, even at 50% radiation dose. SPCCT can more

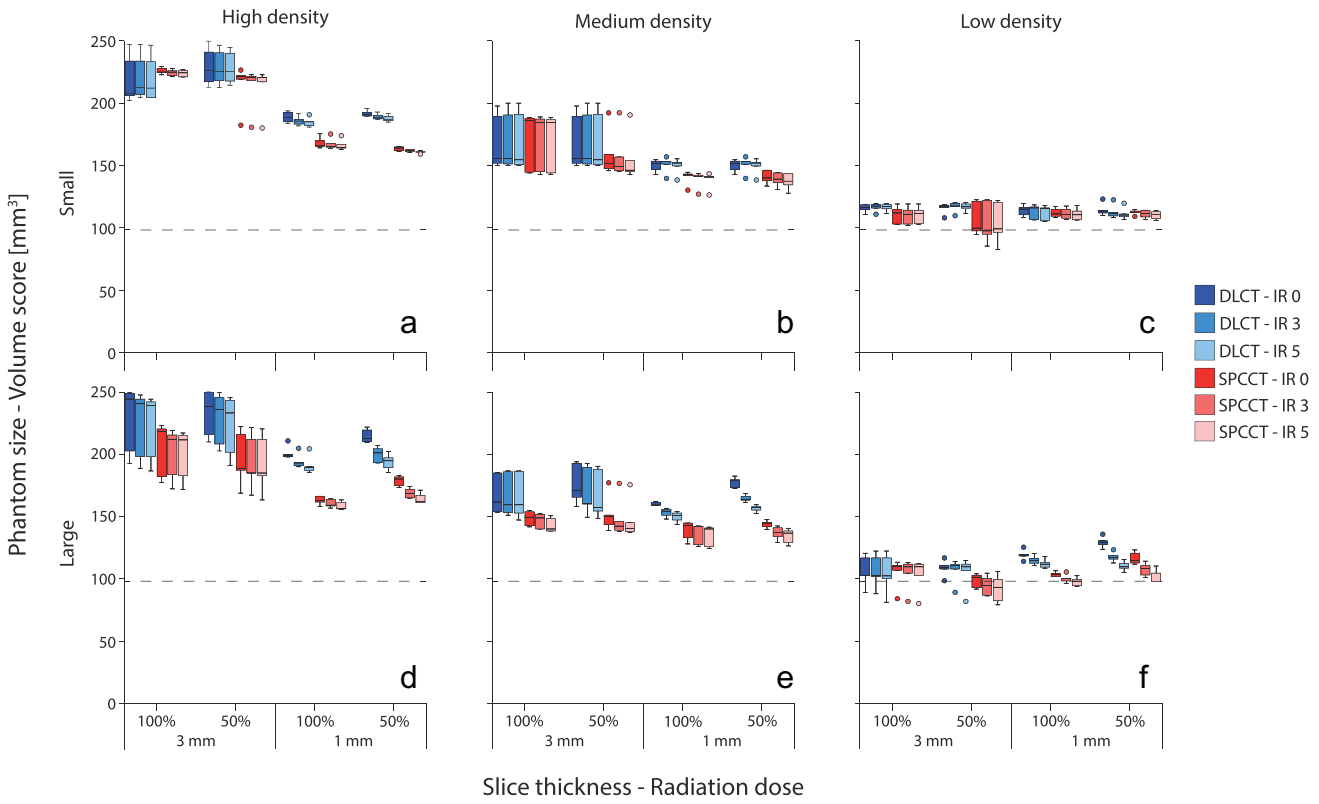

Fig. 3 Box and whisker plots of the volume scores for CCI insert CAC. Results are shown for small (upper) and large (lower) phantom dimensions, high (**a** and **d**)/medium (**b** and **e**)/low (**c** and **f**) CAC density, both CT systems, three IR levels, two slice thicknesses, and both radiation dose levels. The dashed line indicates the total physical volume of the calcifications (96.2 mm^3)

accurately measure physical volumes, especially at reduced slice thickness and for high-density CAC. Both DLCT and SPCCT show more accurate physical mass at reduced slice thickness.

Detection of small and low-density calcifications is clinically relevant, due to the important role of zero CAC scores for the risk estimation of cardiovascular disease [34]. The sensitivity of CT for the detection of small or low-density CAC can be increased by thinner reconstructed slices. However, thinner slices yield an increase in image noise, when radiation dose is kept constant. This can be counteracted by the use of increased levels of IR [35, 36]. The application of IR can, however, impact CAC quantification as CAC can be removed from the image [25, 37–40]. In the current study, CAC detection using SPCCT improved by up to 141% with reduced slice thickness at only 50% of the clinical radiation dose level. For the large phantom size, increased CAC detection of 113% was shown for reduced slice thickness at clinical radiation dose at IR level 3. For both phantom sizes, physical volume approximation improved for large CAC.

To the best of our knowledge, our study is the first to systematically assess CAC detection and quantification at reduced slice thickness and reduced radiation dose for SPCCT systems. Other studies did however assess CAC quantification on SPCCT. Our results corroborate the recent study by Sandstedt et al., who also showed improved CAC volume quantification for SPCCT at standard radiation dose [9]. In that study, however, a SPCCT system with limited FOV was used, and radiation dose reduction was not applied. Also, the exact densities of the used CAC were unknown. Our results are also in-line with a recent publication by Symons et al., who showed improved CAC CNR for SPCCT, which could potentially reduce CAC score radiation dose while maintaining diagnostic image quality [5].

The systematic nature of our study provides insight in CAC detection and the quantification potential of SPCCT for different densities, radiation dose levels, slice thicknesses, and IR levels. Our study also has some limitations. First, a non-commercial SPCCT system was used for our evaluation. Second, our study was based on static phantom data since the rotation gantry rotation time of the used prototype SPCCT system is not optimized yet. Despite the anthropomorphic nature of the phantom with in vivo linear attenuation coefficients, coronary motion and complex internal structures were not taken into account. This could be assessed with a dynamic anthropomorphic phantom in a follow-up study on the next version of the prototype. Using a static phantom did, however, provides us with

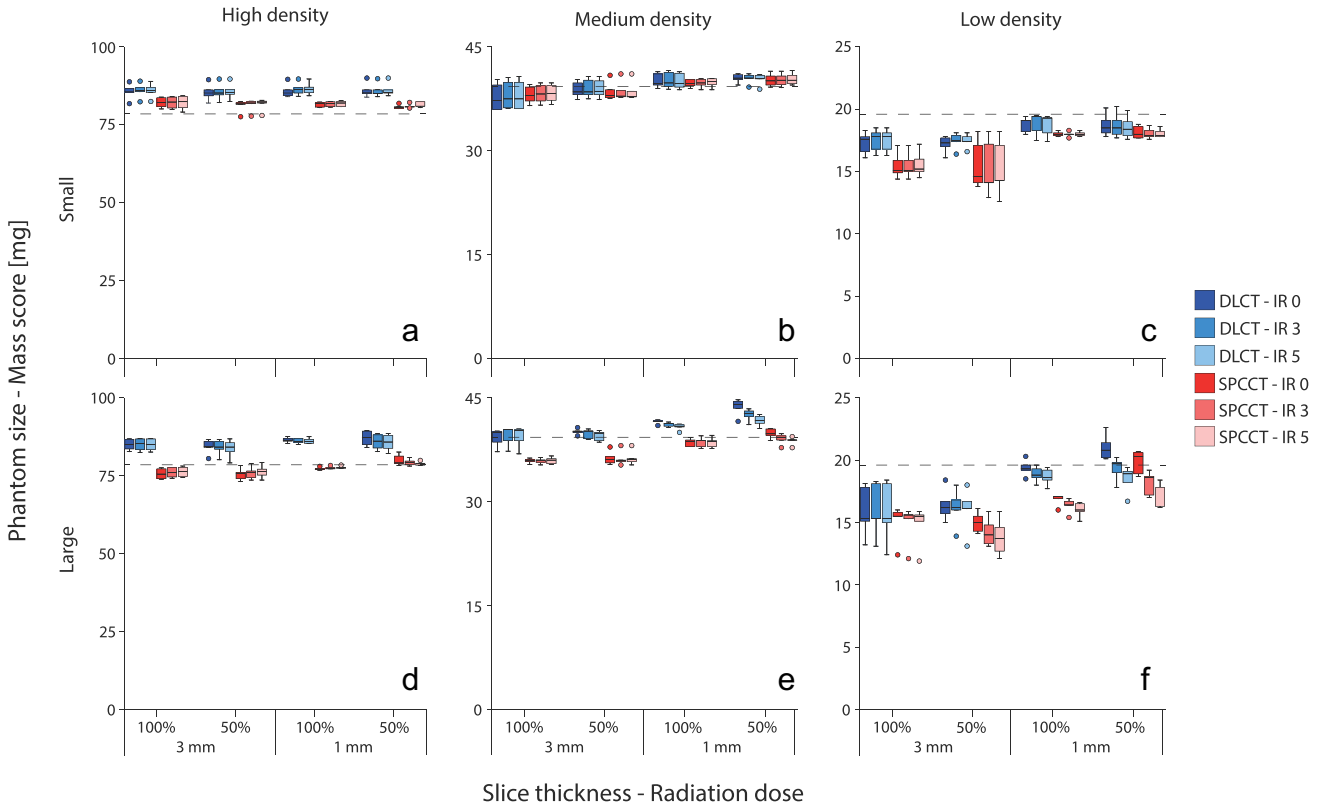

Fig. 4 Box and whisker plots of the mass scores for CCI insert CAC. Results are shown for small (upper) and large (lower) phantom dimensions, high (**a** and **d**)/medium (**b** and **e**)/low (**c** and **f**) CAC density, both CT systems, three IR levels, two slice thicknesses, and both radiation dose levels. The dashed line indicates the total physical mass of the calcifications (78.5, 39.3, and 19.6 mg for high, medium, and low density, respectively)

the opportunity to systematically assess CAC detection, without any influence of motion artefacts. Finally, SPCCT parameters for this study were only based on clinical conventional CT values. Further improvements for SPCCT CAC detection and quantification are likely for SPCCT-specific protocol optimizations.

In conclusion, CAC detection on SPCCT is superior to DLCT, and was even preserved at a reduced radiation dose. Furthermore, SPCCT allows for improved physical volume approximation.

Funding The authors state that this work has not received any funding.

Declarations

Guarantor The scientific guarantor of this publication is Philippe Douek.

Conflict of interest The authors of this manuscript declare no relationships with any companies whose products or services may be related to the subject matter of the article.

Statistics and biometry No complex statistical methods were necessary for this paper.

Informed consent Not applicable

Ethical approval Institutional Review Board approval was not required because this is a phantom-only study.

Methodology

- prospective
- experimental
- performed at one institution

References

1. Sandfort V, Persson M, Pourmorteza A et al (2020) Spectral photon-counting CT in cardiovascular imaging. J Cardiovasc Comput Tomogr. https://doi.org/10.1016/j.jcct.2020.12.005
2. Willemink MJ, Persson M, Pourmorteza A et al (2018) Photon-counting CT: technical principles and clinical prospects. Radiology 289:293–312. https://doi.org/10.1148/radiol.2018172656
3. Leng S, Yu Z, Halaweish A et al (2016) Dose-efficient ultrahigh-resolution scan mode using a photon counting detector computed

tomography system. J Med Imaging 3:043504. https://doi.org/10.1117/1.jmi.3.4.043504
4. Pourmorteza A, Symons R, Henning A et al (2018) Dose efficiency of quarter-millimeter photon-counting computed tomography: first-in-human results. Invest Radiol 53:365–372. https://doi.org/10.1097/RLI.0000000000000463
5. Symons R, Sandfort V, Mallek M et al (2019) Coronary artery calcium scoring with photon-counting CT: first in vivo human experience. Int J Cardiovasc Imaging 35:733–739. https://doi.org/10.1007/s10554-018-1499-6
6. Wang AS, Harrison D, Lobastov V, Tkaczyk JE (2011) Pulse pileup statistics for energy discriminating photon counting X-ray detectors. Med Phys 38:4265–4275. https://doi.org/10.1118/1.3592932
7. Leng S, Gutjahr R, Ferrero A, et al (2017) Ultra-high spatial resolution, multi-energy CT using photon counting detector technology. Proc SPIE Int Soc Opt Eng 139–148. https://doi.org/10.1016/j.physbeh.2017.03.040
8. Mannil M, Hickethier T, Von Spiczak J et al (2018) Photon-counting CT: high-resolution imaging of coronary stents. Invest Radiol 53:143–149. https://doi.org/10.1097/RLI.0000000000000420
9. Sandstedt M, Marsh J, Rajendran K et al (2021) Improved coronary calcification quantification using photon-counting-detector CT: an ex vivo study in cadaveric specimens. Eur Radiol 31:6621–6630. https://doi.org/10.1007/s00330-021-07780-6
10. Budoff MJ, Achenbach S, Blumenthal RS et al (2006) Assessment of coronary artery disease by cardiac computed tomography: a scientific statement from the American Heart Association Committee on Cardiovascular Imaging and Intervention, Council on Cardiovascular Radiology and Intervention, and Committee on C. Circulation 114:1761–1791. https://doi.org/10.1161/CIRCULATIONAHA.106.178458
11. WHO Fact Sheet - The top 10 causes of death. In: May 2018. https://www.who.int/news-room/fact-sheets/detail/the-top-10-causes-of-death. January 2020.
12. Greenland P, Alpert JS, Beller GA et al (2010) 2010 ACCF/AHA guideline for assessment of cardiovascular risk in asymptomatic adults: Executive summary: a report of the American College of cardiology foundation/American Heart association task force on practice guidelines. Circulation 122:2748–2764. https://doi.org/10.1161/CIR.0b013e3182051bab
13. Blaha MJ, Mortensen MB, Kianoush S et al (2017) Coronary artery calcium scoring: is it time for a change in methodology? JACC Cardiovasc Imaging 10:923–937
14. Hecht H, Blaha MJ, Berman DS et al (2017) Clinical indications for coronary artery calcium scoring in asymptomatic patients: expert consensus statement from the Society of Cardiovascular Computed Tomography. J Cardiovasc Comput Tomogr 11:157–168. https://doi.org/10.1016/j.jcct.2017.02.010
15. Agatston AS, Janowitz WR, Hildner FJ, Zusmer NR, Viamonte M Jr, Detrano R (1990) Quantification of coronary artery calcium using ultrafast computed tomography. J Am Coll Cardiol 15:827–832. https://doi.org/10.1016/0735-1097(90)90282-T
16. van der Werf NR, Si-Mohamed S, Rodesch PA et al (2021) Coronary calcium scoring potential of large field-of-view spectral photon-counting CT: a phantom study. Eur Radiol. https://doi.org/10.1007/s00330-021-08152-w
17. McCollough CH, Ulzheimer S, Halliburton SS, Shanneik K, White RD, Kalender WA (2007) Coronary artery calcium: a multi-institutional, multimanufacturer international standard for quantification at cardiac CT. Radiology 243:527–538. https://doi.org/10.1148/radiol.2432050808
18. Callister TQ, Cooil B, Raya SP et al (1998) Coronary artery disease: improved reproducibility of calcium scoring with an electron-beam CT volumetric method. Radiology 208:807–814. https://doi.org/10.1148/radiology.208.3.9722864
19. Hoffmann U, Siebert U, Bull-Stewart A et al (2006) Evidence for lower variability of coronary artery calcium mineral mass measurements by multi-detector computed tomography in a community-based cohort–consequences for progression studies. Eur J Radiol 57:396–402. https://doi.org/10.1016/j.ejrad.2005.12.027
20. Groen JM, Greuter MJ, Schmidt B et al (2007) The influence of heart rate, slice thickness, and calcification density on calcium scores using 64-slice multidetector computed tomography: a systematic phantom study. Invest Radiol 42:848–855. https://doi.org/10.1097/RLI.0b013e318154c549
21. van Ooijen PMA, Vliegenthart R, Witteman JC, Oudkerk M (2005) Influence of scoring parameter settings on Agatston and volume scores for coronary calcification. Eur Radiol 15:102–110. https://doi.org/10.1007/s00330-004-2479-x
22. Ren L, Rajendran K, McCollough CH, Yu L (2019) Radiation dose efficiency of multi-energy photon-counting-detector CT for dual-contrast imaging. Phys Med Biol 64:245003. https://doi.org/10.1088/1361-6560/ab55bf
23. Vonder M, Pelgrim GJ, Meyer M et al (2017) Dose reduction techniques in coronary calcium scoring: the effect of iterative reconstruction combined with low tube voltage on calcium scores in a thoracic phantom. Eur J Radiol 93:229–235. https://doi.org/10.1016/j.ejrad.2017.06.001
24. Vonder M, van der Werf NR, Leiner T et al (2018) The impact of dose reduction on the quantification of coronary artery calcifications and risk categorization: a systematic review. J Cardiovasc Comput Tomogr 12:352–363. https://doi.org/10.1016/j.jcct.2018.06.001
25. van der Werf NR, Willemink MJ, Willems TP et al (2017) Influence of dose reduction and iterative reconstruction on CT calcium scores: a multi-manufacturer dynamic phantom study. Int J Cardiovasc Imaging 33:899–914. https://doi.org/10.1007/s10554-017-1061-y
26. Ode S, Kobayashi Y, Nozu Y, Ogawa Y (2016) The impact of iterative reconstruction on reducing the radiation dose for coronary calcium scoring: an investigation using pulsating calcified coronary phantom. Journal of St. Marianna University 7:95–103
27. Schindler A, Vliegenthart R, Schoepf UJ et al (2014) Iterative image reconstruction techniques for CT coronary artery calcium quantification: comparison with traditional filtered back projection in vitro and in vivo. Radiology 270:387–393. https://doi.org/10.1148/radiol.13130233
28. Willemink MJ, den Harder AM, Foppen W et al (2016) Finding the optimal dose reduction and iterative reconstruction level for coronary calcium scoring. J Cardiovasc Comput Tomogr 10:69–75. https://doi.org/10.1016/j.jcct.2015.08.004
29. den Harder AM, Wolterink JM, Willemink MJ et al (2016) Submillisievert coronary calcium quantification using model-based iterative reconstruction: a within-patient analysis. Eur J Radiol 85:2152–2159. https://doi.org/10.1016/j.ejrad.2016.09.028
30. Sulaiman N, Soon J, Park JK et al (2017) Comparison of low-dose coronary artery calcium scoring using low tube current technique and hybrid iterative reconstruction vs. filtered back projection. Clin Imaging 43:19–23. https://doi.org/10.1016/j.clinimag.2017.01.017
31. McCollough CH, Primak AN, Saba O et al (2007) Dose performance of a 64-channel dual-source CT scanner. Radiology 243:775–784. https://doi.org/10.1148/radiol.2433061165
32. Booij R, van der Werf NR, Budde RPJ et al (2020) Dose reduction for CT coronary calcium scoring with a calcium-aware image reconstruction technique: a phantom study. Eur Radiol 30:3346–3355. https://doi.org/10.1007/s00330-020-06709-9
33. van Praagh GD, van der Werf NR, Wang J et al (2021) Fully automated quantification method (FQM) of coronary calcium in an anthropomorphic phantom. Med Phys 48(7):3730–3740. https://doi.org/10.1002/mp.14912

34. Blaha MJ, Cainzos-Achirica M, Greenland P et al (2016) Role of coronary artery calcium score of zero and other negative risk markers for cardiovascular disease: the Multi-Ethnic Study of Atherosclerosis (MESA). Circulation 133:849–858. https://doi.org/10.1161/CIRCULATIONAHA.115.018524
35. Willemink MJ, Takx RAP, De Jong PA et al (2014) The impact of CT radiation dose reduction and iterative reconstruction algorithms from four different vendors on coronary calcium scoring. Eur Radiol 24:2201–2212. https://doi.org/10.1007/s00330-014-3217-7
36. Takx RAP, Willemink MJ, Nathoe HM et al (2014) The effect of iterative reconstruction on quantitative computed tomography assessment of coronary plaque composition. Int J Cardiovasc Imaging 30:155–163. https://doi.org/10.1007/s10554-013-0293-8
37. Kurata A, Dharampal A, Dedic A et al (2013) Impact of iterative reconstruction on CT coronary calcium quantification. Eur Radiol 23:3246–3252. https://doi.org/10.1007/s00330-013-3022-8
38. Takahashi M, Kimura F, Umezawa T et al (2016) Comparison of adaptive statistical iterative and filtered back projection reconstruction techniques in quantifying coronary calcium. J Cardiovasc Comput Tomogr 10:61–68. https://doi.org/10.1016/j.jcct.2015.07.012
39. Oda S, Utsunomiya D, Nakaura T et al (2017) The influence of iterative reconstruction on coronary artery calcium scoring—phantom and clinical studies. Acad Radiol 24:295–301. https://doi.org/10.1016/j.acra.2016.11.003
40. van der Werf NR, Willemink MJ, Willems TP et al (2017) Influence of iterative reconstruction on coronary calcium scores at multiple heart rates: a multivendor phantom study on state-of-the-art CT systems. Int J Cardiovasc Imaging 0:1–11. https://doi.org/10.1007/s10554-017-1292-y